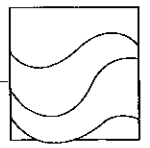

El Niño
Southern Oscillation
New Caledonia

El Niño
Oscillation Australe
Nouvelle Calédonie

ENSO signals in the vicinity of New Caledonia, South Western Pacific

Thierry DELCROIX [a] and Olivier LENORMAND [b]

[a] Groupe SURTROPAC, Institut Français de Recherche Scientifique pour le Développement en Coopération (ORSTOM), BP A5, Nouméa Cedex, New Caledonia.

[b] Centre d'Océanologie de l'Université d'Aix-Marseille II, Campus de Luminy, case 901, F 13288 Marseille Cedex 9, France
et École Supérieure d'Ingénieurs de Marseille (ESIM), Institut Méditerranéen de Technologie, Technopole de Château-Gombert, F 13451 Marseille Cedex 20, France.

Received 28/09/95, in revised form 05/07/96, accepted 12/07/96.

ABSTRACT

Data collected in an area enclosing New Caledonia are analysed both for the open ocean (17°S-27°S, 160°E-170°E; 1972-1992) and for one point in its lagoon (1967-1993), in order to improve our knowledge of the regional environment, with emphasis on seasonal and interannual (*i.e.* ENSO) variability. Long-term means and seasonal changes in surface wind, sea-surface temperature and salinity, and 0-400 m temperature, salinity and zonal geostrophic current are first described to set the context. Through comparisons with the Southern Oscillation Index (SOI), it is demonstrated that there are signals in these parameters that are connected with ENSO. During the warm phase of ENSO (SOI < 0, El Niño), we observed saltier-than-average anomalies in sea-surface salinity (~0.2), 0-50 m cold temperature anomalies (~0.5 °C) contrasting with the well-known warm eastern equatorial Pacific anomalies, together with westerly (~10 m^2 s^{-2}) and southerly (~4 m^2 s^{-2}) wind anomalies over a large part of the studied area. Conversely, anomalies of similar magnitude but of opposite sign were detected during the cold phase of ENSO (SOI > 0; La Niña). The mechanisms which connect these regional anomalies to ENSO evolution at low-latitudes are qualitatively discussed.

RÉSUMÉ

De la signature d'ENSO au voisinage de la Nouvelle Calédonie.

Un ensemble de données, collectées au voisinage de la Nouvelle Calédonie (17°S-27°S, 160°E-170°E) et dans son lagon au cours des 20 à 30 dernières années, est analysé afin d'améliorer notre connaissance de l'environnement régional et de sa variabilité à l'échelle saisonnière et interannuelle (ENSO). Les structures moyennes et les variations saisonnières du vent de surface, de la température de la mer, de la salinité et du courant géostrophique zonal entre 0 et 400 m sont d'abord décrites. Les anomalies liées à ENSO sont ensuite identifiées pour chaque paramètre par comparaison à l'indice d'oscillation australe. Au cours des événements El Niño, la salinité de surface présente des anomalies positives de l'ordre de 0,2, la couche 0-50 m se refroidit d'environ 0,5 °C (contrairement au fort réchauffement observé dans le Pacifique équatorial est), la composante méridienne du vent s'intensifie (~4 m^2 s^{-2}) alors que la composante zonale diminue (~10 m^2 s^{-2}). Les anomalies observées pendant les événements El Niño sont de signes contraires pendant les événements La Niña. Les mécanismes liant les anomalies régionales aux anomalies observées au voisinage de l'équateur sont discutés qualitativement.

Oceanologica Acta, 1997, **20**, 3, 481-491.

INTRODUCTION

The Southern Oscillation (SO) refers to a seesaw in surface pressure anomalies between the Austral-Asian region and the southeastern tropical Pacific. It was first surmised in the work of Hildebrandsson (1897) who evidenced an out-of-phase relationship between surface pressure anomalies at Sydney, Australia, and Buenos-Aires, Argentina. The landmark papers of Walker (1923, 1924) then described the SO-related salient features of surface pressure, temperature and precipitation changes over the tropical Indian and Pacific oceans. Later, a significant new dimension of the SO was provided by Berlage (1966), Bjerknes (1966) and Wyrtki (1975), who documented the remarkable link between interannual Sea Surface Temperature (SST) changes along the Peru and Ecuador coast, previously attributed to the "local" El Niño phenomenon, and the SO-related changes in large-scale precipitation and wind regime. In 1975, Wyrtki postulated that the interannual SST changes in the eastern equatorial Pacific result from a remote response to equatorial winds in the western and central Pacific. Wyrtki's work revealed the dynamic coupling between El Niño and the SO. This ocean-atmosphere coupling was further confirmed by results of equatorial models (McCreary and Anderson, 1991). Nowadays, the label ENSO (El Niño Southern Oscillation) denotes a basin-scale ocean-atmosphere phenomenon.

The tropical regions are the area of the globe most directly affected by ENSO: the associated meteorological and oceanographic changes have been documented for the tropical Atlantic Ocean (*e.g.* Delecluse *et al.*, 1994), for the tropical Indian Ocean (*e.g.* Cadet, 1985), and abundantly for the tropical Pacific Ocean (*e.g.* Rasmusson and Carpenter, 1982). On a global basis, the relationships between ENSO and large-scale precipitation, surface air and sea-surface temperature patterns were discussed by Ropelewski and Halpert (1987), Halpert and Ropelewski (1992) and Trenberth and Hoar (1996). These authors demonstrated that the strongest relationships indeed occur in the tropics, although ENSO signals clearly show up in some sub-tropical regions. In particular, and in contrast with several other regions of the globe, they pointed out that the south central and western Pacific region experiences air and sea-surface temperature anomalies that are out of phase with other regions affected by ENSO. Specifically, in an area extending approximately from 10°S-40°S, 160°E-150°W, the air and sea-surface temperatures appear anomalously cold during warm episodes (El Niño, negative Southern Oscillation Index) and anomalously warm during cold episodes (La Niña, positive SOI).

The south central and western Pacific region, alluded to earlier, is located roughly south of the mean SPCZ (South Pacific Convergence Zone) position and encompasses several island nations and territories, including New Caledonia, Fiji, Vanuatu, part of New Zealand and French Polynesia, all of which suffer economically and ecologically from ENSO effects. In this region, several studies have already highlighted the link between ENSO and regional atmospheric and oceanic anomalies, such as air temperature, rainfall, wind speed and direction, SST, Sea Surface Salinity (SSS), and zonal surface current (*e.g.* Gordon, 1986; Morlière and Rébert, 1986, Delcroix and Hénin, 1989). As a complement to these earlier works, and given the regional ENSO peculiarity, the aim of the present study is to analyse the ENSO signature in the New Caledonia sector. This will be based on extensive observational data sets including SST, SSS, subsurface temperature and salinity profiles and surface wind.

The organization of the paper is as follows. In the next section, the data and data processing will be presented. Then, long-term averages will be discussed in order to set the context, and seasonal changes will be examined since they generally account for a large part of the variability in sub-tropical regions; this section also provides a convenient summary of the knowledge gained from past regional studies. In the following section, emphasis will be put on ENSO-related anomalies in order to identify the signature of ENSO, if any, upon the analysed parameters. Conclusion and discussion will be given in the last section.

DATA AND DATA PROCESSING

The oceanic surface measurements (SST and SSS) were derived from sea-water samples collected as part of an ORSTOM ship-of-opportunity programme (SOP) operated from Nouméa, New Caledonia, since 1969 (see the article by Donguy, 1987, and its references). Although quoted as "surface" measurements, it should be noted that the SST and SSS data are in fact representative of the water layer between the surface and about 8 m, depending on the ship draft and load. The ORSTOM-SOP measurements have already been used in the literature, for example, in the analysis of seasonal and interannual variations of SSS and SST in the tropical Pacific (Delcroix and Hénin, 1991; Delcroix, 1993). As detailed in these last references, measurements of SST and SSS are routinely validated before entering the ORSTOM data base, through procedures that check for flagrant errors, internal consistency of data pertaining to each voyage and climatic limits. The expected accuracy of a given measurement is of the order of 0.1 for SSS and of 0.3 °C for SST.

In the vicinity of New Caledonia (17°S-27°S, 161°E-171°E; Fig. 1*a*), the ORSTOM-SOP collected about 12,000 SST and SSS data during the 1972-1992 period. Details concerning the time-space distribution of these data are given in Lenormand (1995). Following the routine subjective validation, additional validation tests were applied to the selected values of Figure 1*a*. Spurious measurements were detected through objective criteria based on multiples ($\pm$ 5, $\pm$ 4, and $\pm$ 3.5) of sample standard deviations computed in 1° latitude bands. The resulting assumed spurious measurements (< 1%) were rejected. Based on the validated data, maps of the long-term mean SST and SSS (1972-1992) are displayed in Figure 2*a*, *b*; they will be discussed in the following section. At this stage, we note that the spatial SST and SSS changes are generally greater in the meridional than in the zonal direction.

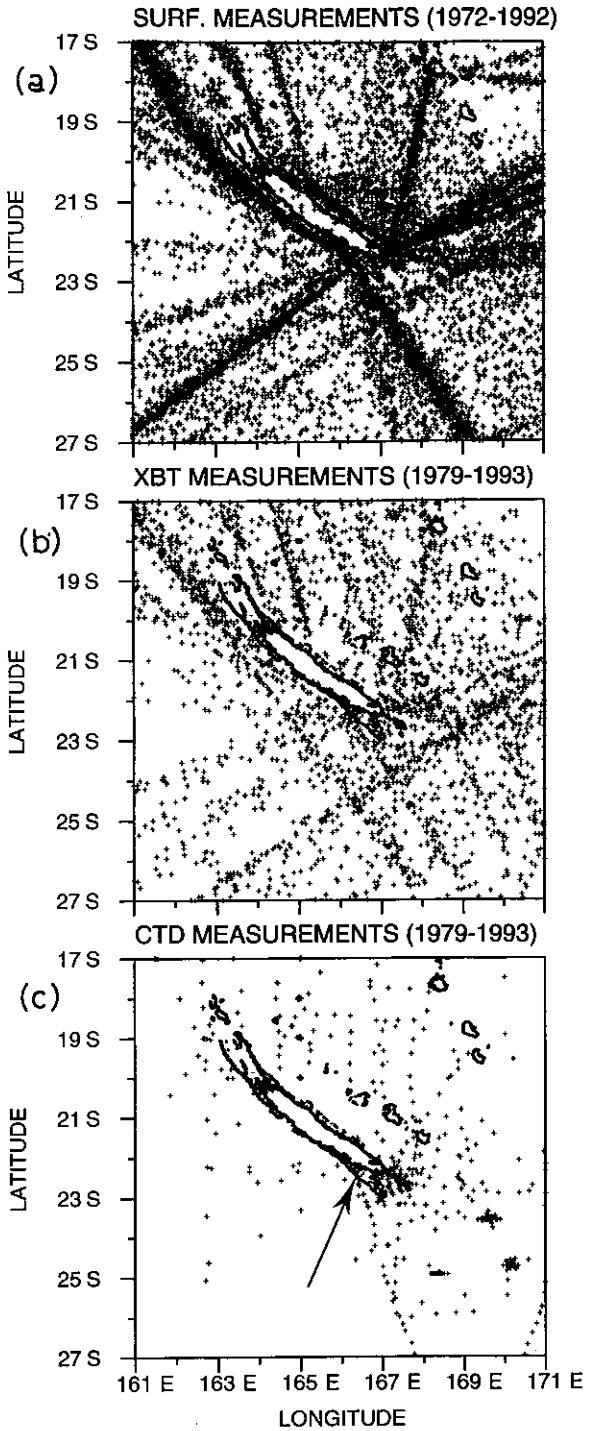

Figure 1

Spatial distribution of (a) sea-surface temperature and salinity, (b) XBT, and (c) subsurface temperature and salinity measurements collected in the vicinity of New Caledonia during the reported time periods. The arrow in (c) indicates the location of the Amédée Lighthouse.

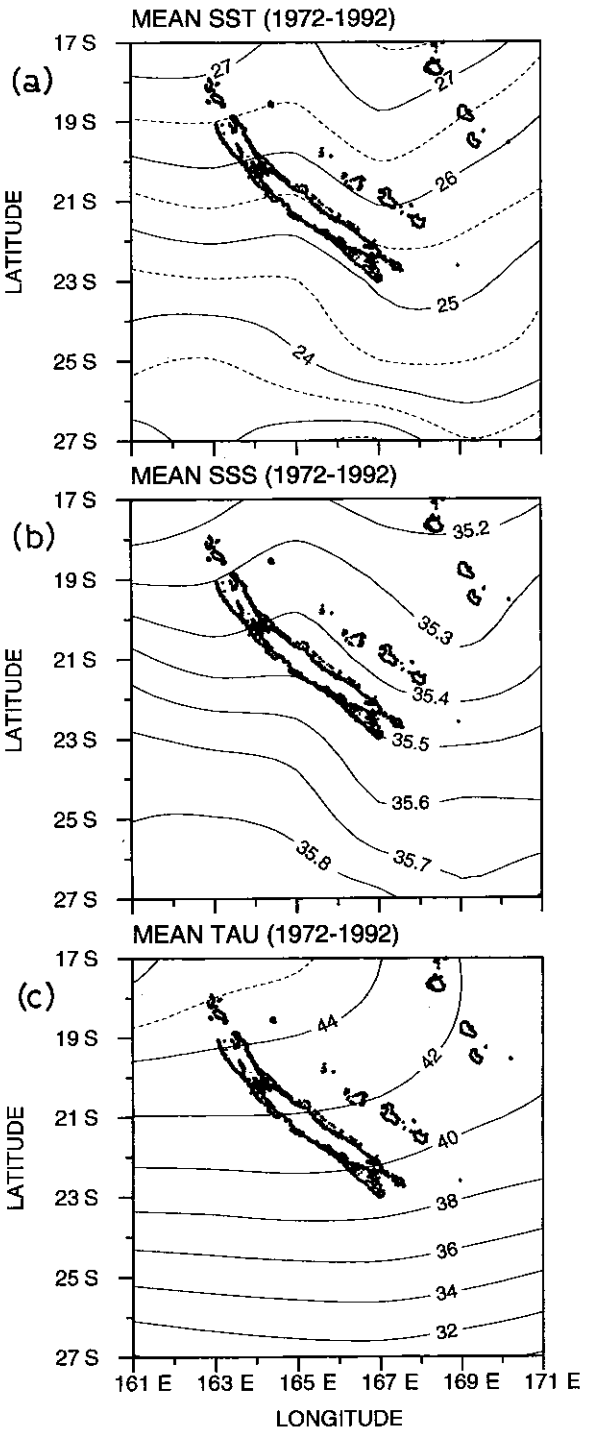

Figure 2

Mean (a) sea-surface temperature, (b) sea-surface salinity, and (c) pseudo wind stress modulus. Units are °C and $m^2\ s^{-2}$ in (a) and (c), respectively. All values are averaged over the 1972-1992 period.

In order to analyse changes in SST and SSS fields, the irregularly-distributed longitude-latitude-time SST and SSS data were interpolated (or averaged, as appropriate) on to a regular 1-month by 1°-latitude grid, from 27°S to 17°S and from January 1972 to December 1992. This was performed through an objective interpolation scheme (Laplacian method), in a manner similar to Delcroix and Hénin (1991).

This latitude-time gridding procedure was done ignoring the longitude of measurements within 161°E-171°E, on the grounds that the information lost does not severely bias the gridded fields given the tendency for meridional gradients to dominate zonal gradients (Fig. 2*a*, *b*) and the 15° zonal decorrelation scale in SST (White *et al.*, 1985). On an average, a gridded value represents 4.3 observations collected during a given month, within a 1° latitude band and within 161°E-171°E longitude. The rms error is thus

roughly reduced by $4.3^{1/2}$ and we believe that the overall accuracy of one gridded value is better than 0.1 for SSS and 0.3 °C for SST.

A more comprehensive SST and SSS data set is available at Amédée Lighthouse (22°29'S-166°28'E) which is located in the lagoon close to a pass through the reef barrier, about twelve nautical miles south of Nouméa, New Caledonia (*see* Fig. 1*c*). Such a data set enables us to compare open-ocean and lagoon waters as far as seasonal and ENSO signals are concerned. It consists of daily observations taken between 5 and 9 AM during the period 1967-1994. When necessary, values of SST have been extrapolated to 7 AM based on a mean diurnal cycle which indicates an almost-linear increase of 0.1 °C per hour between 5 AM and 3 PM (C. Hénin, pers. comm., 1995). Seven-day median and Hanning filters (Bendat and Piersol, 1971) were applied to the daily SST and SSS time series to suppress high-frequency variations, and the filtered values were monthly averaged.

Regarding subsurface measurements, about 3800 temperature and 610 salinity profiles were collected in the studied region during the 1979-1993 period. The temperature profiles were obtained from eXpendable BathyThermograph (XBT, 83%), hydrocast and Conductivity Temperature Depth (CTD) measurements (Fig. 1*b*, *c*), the latter providing the salinity profiles. The XBT drops were made from ships-of-opportunity along shipping routes (Meyers and Donguy, 1980) and the two other types of measurements originate from 53 research cruises carried out by ORSTOM scientists. In combining XBT, hydrocast and CTD profiles, the XBT depths were multiplied by a correction factor (C = 1.0336) to account for the new depth equation for XBT (Hanawa *et al.*, 1994).

The temperature and salinity profile data were submitted to a validation test similar to the one performed for SST and SSS. For each profile, temperature and salinity were first linearly interpolated at intervals of 5 m, from the surface down to 400 m. Then, at each level, spurious values were detected through standard deviation criteria ($\pm$ 5, $\pm$ 4, and $\pm$ 3.5) over 2° latitude bands. Out of the complete file, 6.5% of the profiles were rejected. The irregularly-distributed longitude-latitude-time temperature values were interpolated (or averaged, as appropriate) on to a regular 1-month by 2°-latitude by 5 m depth grid, following the technique detailed in Delcroix and Hénin (1991). On average, each grid point represents 3.3 temperature measurements collected during a given month (from January 1979 to December 1993), within a 2° latitude band (from 27°S to 17°S), within a 5 m depth interval (from 0 to 400 m) and within 161°E-171°E longitude. This gridding procedure was not possible for the salinity profiles given the poor time-space distribution: only the long-term mean latitude-depth salinity will be discussed in the following section.

As for surface winds, they are derived from the monthly Florida State University (FSU) pseudo-stress fields which are available on a 2° latitude by 2° longitude grid over the tropical Pacific (Goldenberg and O'Brien, 1981). Monthly values from January 1972 to December 1992, from 17°S to 27°S and averaged within 160°E-170°E longitude were used to derive 1-month by 2° latitude grids of pseudo-stress moduli (hereafter referred to as $|\tau|$), zonal pseudo-stress (τ^x), and meridional pseudo-stress (τ^y) in $m^2\ s^{-2}$ unit.

MEANS AND SEASONAL VARIATIONS

Maps of long-term mean SST, SSS and $|\tau|$ (1972-1992) are displayed in Figure 2*a*, *b*, *c*. The mean SST increases equatorward from about 23 °C at 27° S latitude to 27.5 °C at 17° S. The surface isotherms are almost zonally oriented with, however, about 0.5 °C difference at the same latitude between the western and eastern side of New Caledonia (east being warmer). In contrast to the mean SST, the mean SSS decreases equatorward from about 35.8 at 27°S latitude to 35.2 at 17°S. The surface isohalines are also almost zonally oriented with again a small difference (< 0.1) between the eastern and western sides of New Caledonia (east being fresher). It is worth noting that the 35.4 isohaline and 25.5-26 °C isotherm parallel the eastern coast of New Caledonia's main island, reflecting the likely role of advection by the coastal *Courant du Vauban* which flows south-eastward between the main island and the Loyalty Islands (Hénin *et al.*, 1984, 1995). The average direction of the wind (not shown here) is E-SE, reflecting the dominance of the trade winds in the region. The mean pseudo-stress modulus ranges from less than 32 $m^2\ s^{-2}$ at 27°S latitude to 41-46 $m^2\ s^{-2}$ at 17°S. It is virtually unaffected by longitude in the southern half of the region, but increases westward in the northern half. The tendency for $|\tau|$ to be weaker in the east than in the west of New Caledonia is consistent with the tendency for SST to be warmer and for SSS to be fresher in the east than in the west, reflecting the possible effects of evaporative cooling, wind mixing and evaporation.

Mean monthly values in SST, SSS, and $|\tau|$, averaged over the 161°E-171°E band, are displayed in Figure 3*a*, *b*, *c* between 27°S and 17°S latitudes (*see* also Hénin, 1982). The warm water pool (SST > 28 °C) of climatic significance (Lukas and Webster, 1992) penetrates south of 19°S for about three months, reaching the latitude of Port-Vila, Vanuatu, from January to April. As expected, the SST is warmest (coldest) in February-March (August-September), *i.e.* by the end of the austral summer (winter), reflecting the remarkable effect of surface thermal forcing in governing extra-equatorial SST. As discussed below, the annual variations of SST are the dominant features since they represent more than 80% of the total variance.

The mean monthly values in SSS (Fig. 3*b*) present relatively strong changes in the northern *versus* the southern part of the region. Maximum (minimum) SSS takes place around September (March) from 17°S to 27°S, with an annual amplitude of the order of 0.15 at 17°S latitude, decreasing to almost-zero at 27°S. Looking at the northern part of the region only, the seasonal SSS cycle is out of phase with the seasonal precipitation cycle (*see* Morlière and Rébert, 1986; Lenormand, 1995) and in phase with the seasonal $|\tau|$ cycle (Fig. 3*c*). Namely, the September maximum in SSS roughly corresponds to a minimum in precipitation and to a minimum in $|\tau|$, suggesting the

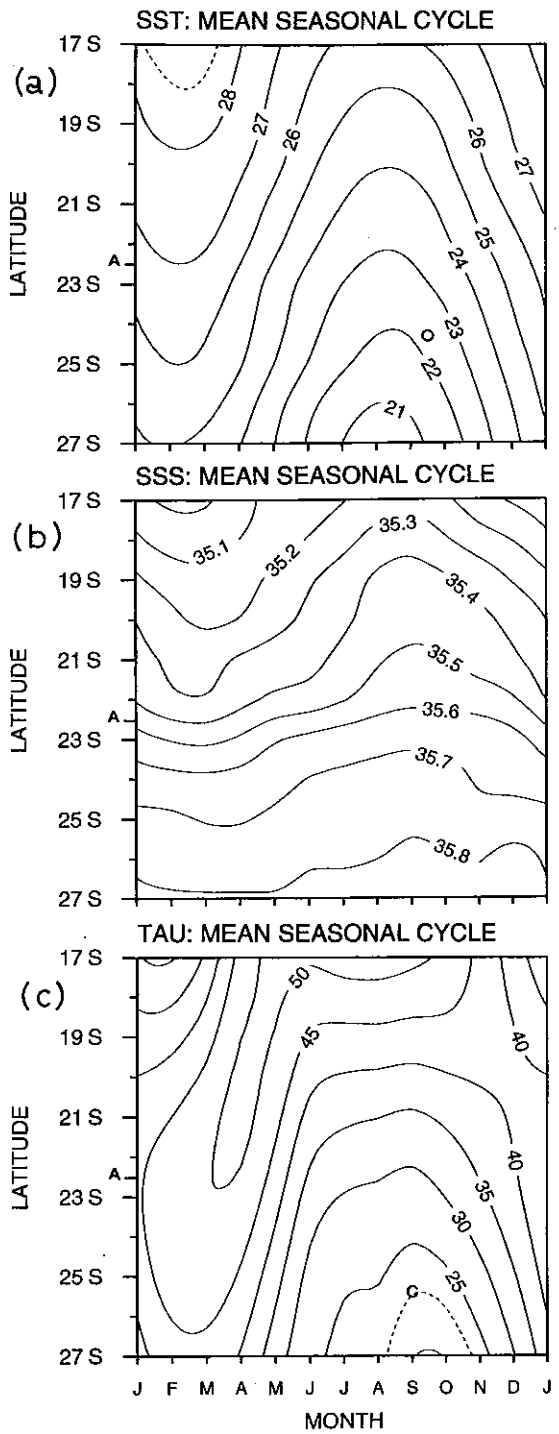

Figure 3

Mean monthly values of (a) sea-surface temperature, (b) sea-surface salinity, and (c) pseudo wind stress modulus. Units are °C and m^2 s^{-2} in (a) and (c), respectively. All values are averaged over 1972-1992 and within 160° E-170° E. The letter "A" in the vertical axis indicates the latitude of the Amédée Lighthouse.

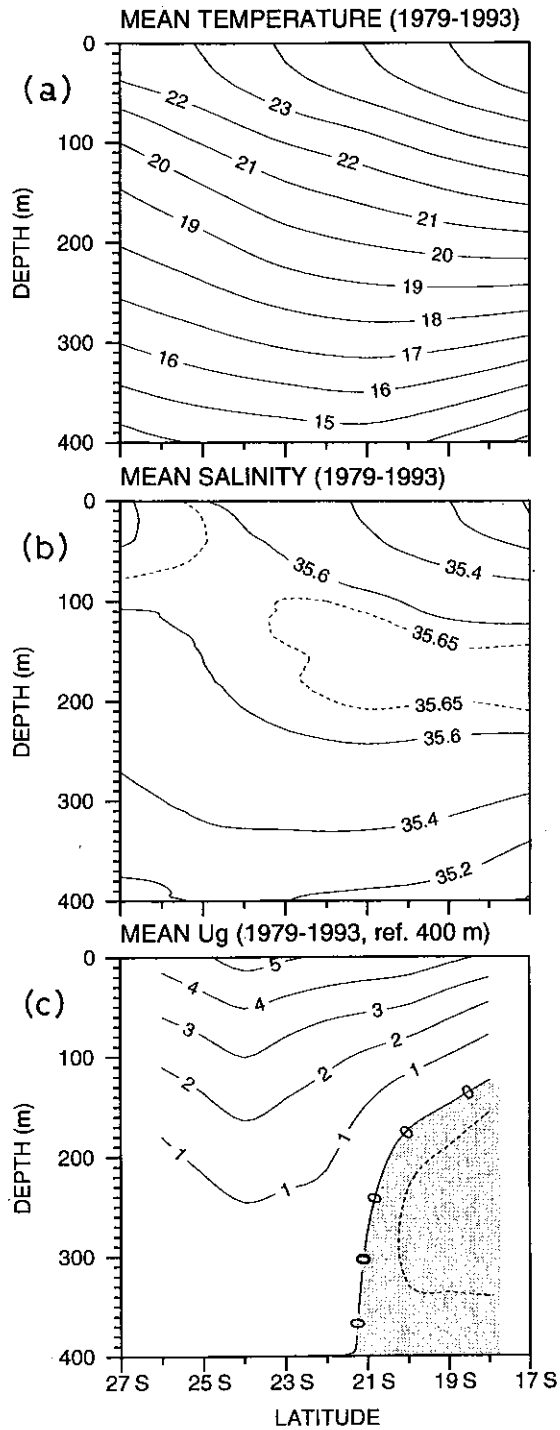

Figure 4

Mean latitude-depth distributions of (a) temperature, (b) salinity, and (c) zonal geostrophic current relative to 400 m. Units are °C and cm s^{-1} in (a) and (c), respectively. Negative (shaded) current denotes westward flow. All values are averaged over 1979-1993 and within 160° E-170° E.

combined role of evaporation and precipitation (P) in modulating SSS. Contrary to SST, it should be noted that the annual SSS, P and $|\tau|$ cycles represent less than 20, 30 and 40% of the total variance, respectively (Lenormand, 1995).

As mentioned in the section above, a longer and finer resolution SST and SSS data set has been collected at the Amédée lighthouse, in the lagoon off Nouméa. At the Amédée lighthouse, on the average, the lagoon waters are about 1.5 °C colder and 0.2 saltier than in the open ocean (Table 1, Fig. 2), in agreement with a similar comparison mentioned by Hénin *et al.* (1984). Seasonal change in SST ranges from 25.8 °C in March to 21.0 °C in August, with monthly standard deviations of the order of 0.6 °C

Table 1

Monthly means, annual mean and standard deviations (σ) for Sea Surface Temperature (SST) and Salinity (SSS) at Amédée Lighthouse (22°29'S, 166°28'E). Values are based on daily measurements made during the 1967-1994 period for SST and 1974-1994 for SSS.

	Jan.	Feb.	Mar.	Apr.	May	June	July	Aug.	Sept.	Oct.	Nov.	Dec.	Mean
SST	25.6	25.6	25.8	24.6	23.4	22.4	21.4	21.0	21.4	22.5	23.6	24.6	23.5
σ_{SST}	0.6	0.7	0.7	0.7	0.5	0.5	0.4	0.5	0.6	0.6	0.7	0.7	1.7
SST	35.7	35.6	35.5	35.6	35.7	35.7	35.8	35.8	35.9	35.9	35.8	35.8	35.7
σ_{SSS}	0.3	0.3	0.3	0.3	0.2	0.2	0.2	0.2	0.2	0.2	0.2	0.2	0.2

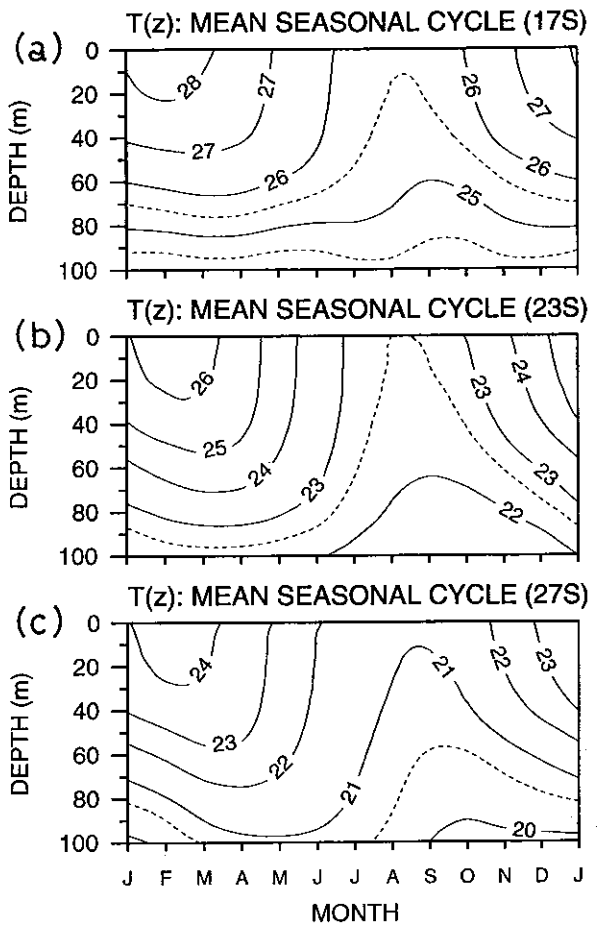

Figure 5

Mean monthly values of temperature (°C) as a function of depth, for three selected latitudes, (a) 17°S, (b) 23°S, and (c) 27°S. Monthly values have been calculated from data collected during 1979-1993 and within 160°E-170°E.

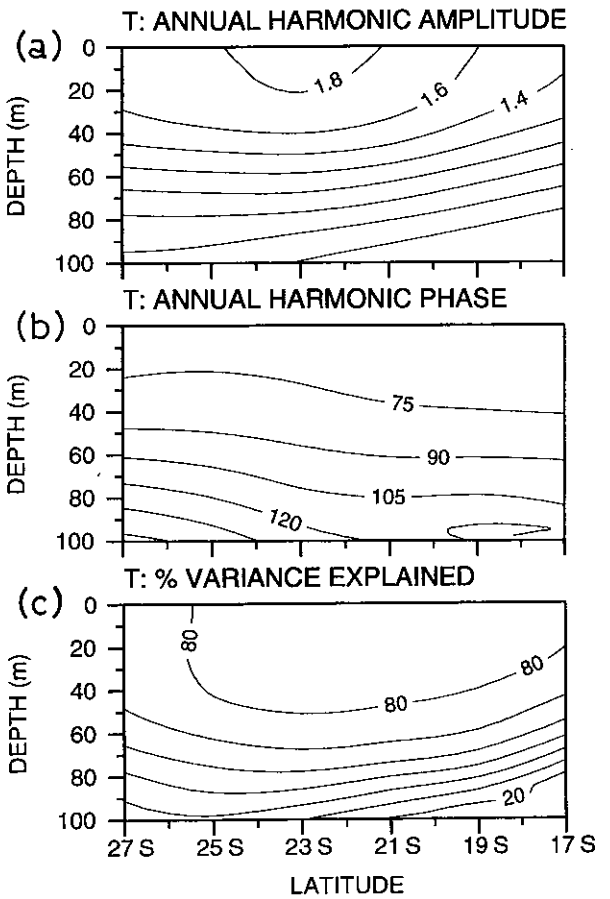

Figure 6

Annual harmonic of 160°E-170°E averaged temperature as a function of latitude and depth: (a) amplitude (°C), (b) year-day phase of warmest sea-surface temperature, and (c) per-cent of total variance explained by the annual harmonic.

(Table 1). Seasonal change in SSS ranges from 35.5 in March to 35.9 in October, with monthly standard deviations of the order of 0.2-0.3. The amplitude of the seasonal variations is thus similar in magnitude inside and outside the lagoon for SST, and twice as much for SSS (Table 1, Fig. 3). The origin of the differences between the lagoon and open-ocean waters is unclear. It may reflect river runoff, local upwelling (the trade winds parallel the reef), strong vertical mixing close by the reef, and/or enhanced evaporation due to the existence of diurnal wind: all these processes but river runoff would consistently bring colder and saltier water close by the reef.

We now turn our attention to subsurface measurements. The 1979-1993 mean latitude-depth distributions of temperature and salinity, averaged over the 161°E-171°E band, are displayed in Figure 4*a,b*, together with the derived zonal geostrophic current relative to 400 m (Fig. 4*c*). In the northern part of the region, deepening of the upper isotherms (> 19 °C) and rising of the lower isotherms characterize the appearance of the equatorial thermocline found farther to the north. This spreading of isotherms reflects a 0-150 m eastward geostrophic current flowing above a weak westward current characterizing the southern edge of the South Equatorial Current. The zero isothach located at 21°S below 200 m reaches the surface near 15°S

(*see* Delcroix and Hénin, 1989, their Fig. 10), it denotes the large-scale South Pacific anticyclonic gyre axis. In the southern part of the region, an almost-constant vertical temperature gradient (2.3×10^{-2} °C.m^{-1}) can be seen on Figure 4*a*, with all the isotherms rising toward the surface. This upward movement of isotherms induces a 0-400 m eastward geostrophic current: it was referred to as the South Tropical Countercurrent (Merle *et al.*, 1969) and characterizes the northern side of the eastward flow which extends as far as the Antarctic Circumpolar Current. Figure 4*b* shows a low salinity water (S < 35.4) near the surface equatorward of 21°S, above a tongue of high salinity (S > 35.65) located around 160 m, in agreement with the results of Rougerie and Donguy (1975). The high salinity water characterizes the south Pacific tropical water formed further east in the vicinity of French Polynesia (Wyrtki, 1962). High salinity waters are also found near the surface south of 25°S; they partly originate from intrusions of Bass Strait waters into the Tasman Sea (Tomczak, 1981).

Mean monthly values of 0-100 m temperature are displayed in Figure 5*a*, *b*, *c* for three selected latitudes, 17°S, 23°S and 27°S. (Note that 100-400 m temperature and 0-400 m zonal geostrophic current are not discussed here because the seasonal changes are very weak.) Significant seasonal cycles exist in the first 100 m with the warmest temperature in February/March at the surface and progressively later in the year at depth (*e.g.* in May-June at 100 m, 27°S). For the three selected latitudes, Figure 5*a*, *b*, *c* shows the development of a seasonal thermocline in summer and, *a contrario*, a well-mixed temperature layer in winter. Through a Fourier analysis, computation of the annual harmonic enabled us to assess how representative was the annual temperature cycle out of the total temperature signal. The amplitude and phase (*i.e.* year-day phase of warmest temperature) of the annual harmonic, together with the percent of variance explained by the annual harmonic are shown in Figure 6*a*, *b*, *c* as a function of depths and latitudes. The annual amplitude of 1.4-1.8 °C near the surface, accounting for more than 80 % of the total variance, declines rapidly to less than 0.5 °C at 100 m depth where it represents 20 to 40% of the total variance. The date of the annual temperature maximum is delayed with depth, from mid-March (day 75) in the upper 30 m to early May (day 120) at 100 m. All the above patterns characterize a mid-latitude open ocean where an ENSO signal is not generally seen.

THE SIGNATURE OF ENSO

Bearing in mind this overview of the average conditions and of the seasonal changes, we then asked ourselves the following question: what is the signature of ENSO, if any, on the analysed surface and subsurface parameters? To answer this question, we calculated monthly anomalies relative to the long-term means (1972-1992 for the surface parameters; 1979-1993 for the subsurface temperature), and we filtered the resulting time series in time with a 12-month Hanning filter (half length) in order to remove annual and shorter-period variations. The potential impact of ENSO was examined by comparing the interannual anomalies and the SOI which was also filtered with a 12-month Hanning filter. The comparison was guided by lagged correlation analysis.

The interannual anomalies of SST, SSS, and τ^y (1972-1992, 17°S-27°S) are shown in Figure 7*a*, *b*, *c*, together with the SOI in Figure 7*d*. Periods of warm (cold) SST anomalies of the order of 0.5 °C have a clear tendency to appear during La Niña (El Niño) events when the SOI is positive (negative). Namely, the warm SST anomalies occur during the 1973-1975 (not in the southern half of the region in 1973-74) and 1988-1989 La Niña and, conversely, the cold SST anomalies occur during the 1982-1983, 1987 and 1991 El Niño (not during the 1977 El Niño). Such correspondence still applies between SSS anomalies and the SOI. Fresher-than-average (saltier-than-average) SSS anomalies ranging within 0.1-0.3 are clearly associated with La Niña (El Niño) events over almost the full latitudinal range. Of particular interest in this regard is the penchant for the peak SSS anomalies, regardless of the sign, to arise a few months after the SOI peak, with the time delay increasing with latitude. The meridional pseudo-stress anomalies (τ^y) are also related to the SOI, in agreement with the results of Van Loon and Shea (1985). Southerly wind anomalies coincide to a large extent with El Niño episodes in 1972, 1977, 1982-1983, 1987, and 1991-1992, and northerly anomalies are observed during the two La Niña periods in 1973-1975 and 1988. The zonal pseudo-stress (τ^x) and pseudo-stress modulus ($|\tau|$) anomalies are consistent with the SOI mainly north of 19°S latitude (not shown here; *see* Lenormand, 1995), with magnitudes of the order of -5 and $+5$ m^2 s^{-2} during El Niño events, respectively; the signs of the anomalies are reversed during La Niña events.

Tables 2 and 3 present the zero-lag and maximum correlation between the SST, SSS, $|\tau|$, τ^y, and τ^x anomalies and the SOI. In addition to the preceding qualitative comparisons, it appears that the observed anomalies in SST and pseudo-stresses are significantly correlated with the SOI in the northern part of our domain, at almost zero-lag, with values ranging in magnitude between 0.43 and 0.85. Regarding SSS anomalies, they also are significantly correlated with the SOI but now over the full domain (R < −0.7). Furthermore, as noted previously, SSS anomalies seem to migrate southward with 8-month delay at 17°S and 13-month delay at 27°S as compared to the SOI. Thus, not all but a significant part of the interannual variability in the surface parameters is related to ENSO.

The relationships between SST and SSS anomalies still exist at the Amédée lighthouse, inside the New Caledonian lagoon. Cold (warm) SST anomalies and saltier-than-average (fresher-than-average) SSS anomalies clearly have a propensity for arising during warm El Niño (cold La Niña) episodes (Fig. 8), with magnitude similar to, or greater than, that which is observed in the open ocean (Fig. 7*a*, *b*). Specifically, we note the very contrasted SSS conditions encountered in 1989 during La Niña and in 1992 during El Niño, with peak-to-peak values reaching as much as 0.7. Such extremes are of major interest and probably

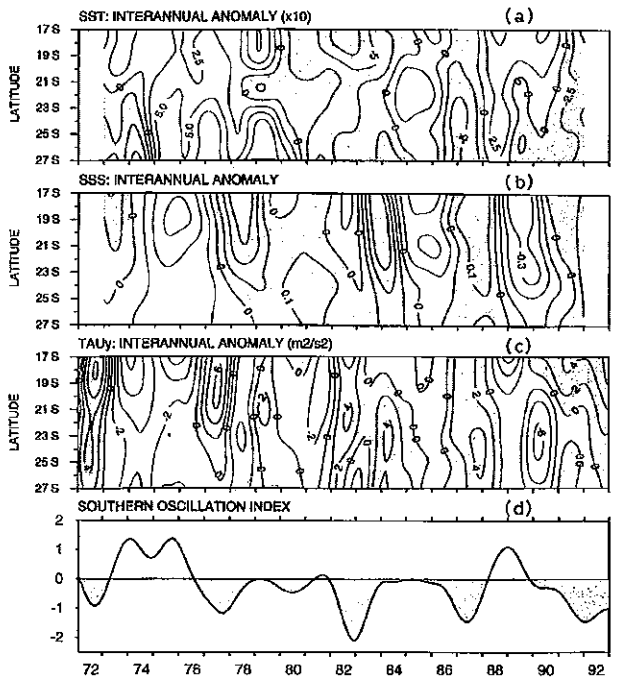

Figure 7

Interannual anomalies of 160°E-170°E averaged (a) sea-surface temperature (°C × 10), (b) sea-surface salinity, and (c) meridional pseudo-stress ($m^2\ s^{-2}$; positive to the north). All values are relative to the 1972-1992 period. The bottom panel (d) represents the Southern Oscillation Index which is filtered in time with a 12-month Hanning filter. Shaded areas indicate negative anomalies in (a) and (d), and positive anomalies in (b) and (c).

of concern for local fishing and aquaculture activities. For the time series as a whole, SST and SSS anomalies *versus* the SOI are highly correlated with values of 0.61 (3-month lag) and 0.66 (9-month lag), respectively (Table 2) (note that the zero-lag correlation for SST is 0.57 which is not statistically different from 0.61). Hence, the ENSO signal does exist inside the New Caledonian lagoon. Moreover, we observe a cooling trend of −0.4 °C over 10 years. Such a trend is also detected in open-ocean measurements (−0.3 °C over 10 years within 17°S-27°S), and may be related to the excess of positive versus negative SOI in the first half of the analysed period as compared to the excess of negative *versus* positive SOI in the second half.

Table 2

Simultaneous (R_0) and maximum (R_1) correlations (× 100) at given lag (months) between interannual anomalies of sea-surface temperature (SST) and sea-surface salinity (SSS) versus *the Southern Oscillation Index (SOI). A positive lag indicates that the SOI leads the anomalies. SST and SSS anomalies between 17°S and 27°S are averaged within 161°E-171°E. The Amédée Lighthouse is located at 22°29'S-166°28'E. Only correlations significantly different from zero at 95% confidence level are reported.*

Location	SST			SSS		
	R_0	R_1	lag	R_0	R_1	lag
17°S	55	55	− 1	− 43	− 74	8
18°S	54	54	0	− 43	− 78	8.5
19°S	43	43	0	− 47	− 82	9
20°S	58	58	− 1		− 79	10
21°S					− 77	10
22°S					− 78	11
23°S	43	43	0		− 71	12
24°S					− 69	13
25°S					− 73	14.5
26°S					− 71	13
27°S				− 45	− 72	13
Amédée Lighthouse	57	61	− 3	− 36	− 66	9

We then focused our attention on subsurface temperatures which are available over 15 years, from 1979 to 1993. Despite the length of the time series, it is rather short to test for significant correlations between interannual anomalies and the SOI. In fact, the Hanning filter used to derive interannual anomalies reduces the number of effectively independent values and further diminishes the time series by two years (1979 and 1993). Basically, the time between independent values is about one year and only correlation coefficients greater than 0.5 are significantly non-zero at the 95% level of confidence. With this caveat in mind, Figure 9 presents the latitude-depth distribution of zero-lag correlation coefficients between the interannual temperature anomalies and the SOI. The positive sign of correlations confirms that cold anomalies emerge during warm El Niño events (SOI < 0), whereas warm anomalies come out during cold La Niña events (SOI > 0). These points underline once again that regional temperature anomalies

Table 3

Simultaneous (R_0) and maximum (R_1) correlations (× 100) at given lag (months) between interannual anomalies of pseudo wind stress modulus ($|\tau|$), zonal pseudo wind stress (τ^x), meridional pseudo wind stress (τ^y) versus *the Southern Oscillation Index (SOI). A positive lag indicates that the SOI leads the anomalies. $|\tau|$, τ^x and τ^y anomalies are averaged within 160°E-170°E. Only correlations significantly different from zero at 95% confidence level are reported.*

Location	$\|\tau\|$			τ^x			τ^y		
	R_0	R_1	lag	R_0	R_1	lag	R_0	R_1	lag
17°S	− 67	− 67	0	53	53	1	− 85	− 85	0
19°S	− 60	− 60	1	44	46	2	− 77	− 77	0
21°S							− 61	− 61	0
23°S							− 46	− 46	0
25°S									
27°S									

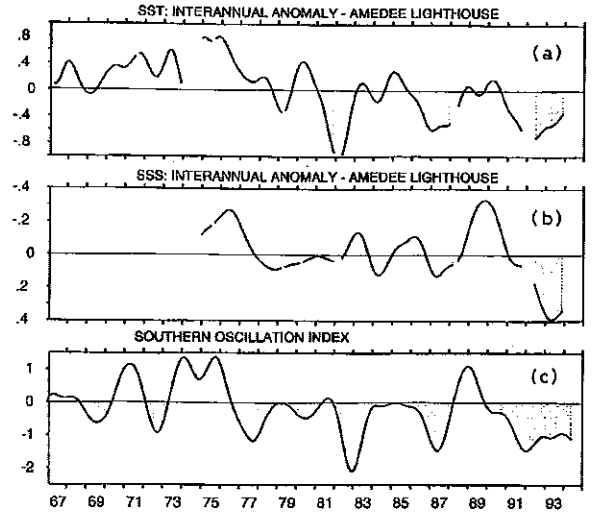

Figure 8

Interannual anomalies of 160°E-170°E averaged (a) sea-surface temperature (°C), and (b) sea-surface salinity at the Amédée lighthouse (22°29'S, 166°28'E). All values are relative to the respective duration of the time series. The bottom panel (c) represents the Southern Oscillation Index which is filtered in time with a 12-month Hanning filter. Shaded areas indicate negative anomalies in (a) and (c), and positive anomalies in (b).

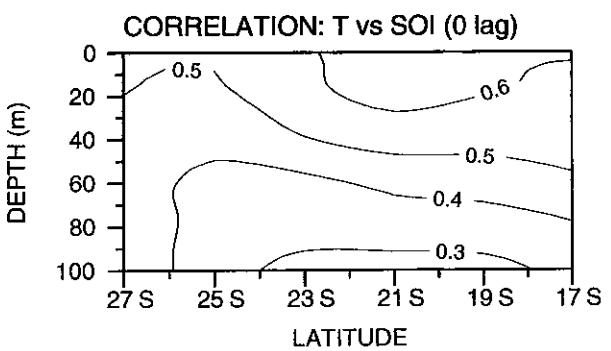

Figure 9

Latitude-depth distribution of zero-lag correlation coefficients between the Southern Oscillation Index, filtered in time with a 12-month Hanning filter, and the interannual anomalies of 160°E-170°E averaged temperature over the 1979-1993 period. Values greater than 0.5 are significant at 95%.

are out of phase with those in the eastern and central equatorial Pacific. It is worth noting that the correlations are maximum at zero-lag in the 0-100 m layer (this is not true below 100 m where the correlations are not significant), and their values at the surface are similar to those obtained with bucket measurements (Table 2). Quantitatively, the magnitude of the temperature anomalies (not shown here) associated with ENSO ranges from about 0.5 °C at the surface, as in Figure 7 for SST, to almost-zero below 100 m depth. Figure 9 indicates clearly that ENSO-related temperature anomalies appear mainly in the near surface, decreasing regularly with depth. We shall return to the implications of this result in the following section.

Time series of zonal geostrophic current relative to 400 m were calculated at each latitude and depth, using the 0-400 m temperature time series and mean T-S curves (*see* Figure 4*a,b*). In the absence of salinity time series below the surface, it is worth pointing out that this T-S procedure neglects the strong ENSO-related salinity changes as identified in Figure 7*b* for SSS. Combined with the assumption that 400 m can be meaningfully used as a reference level, the resulting error is of the order of $\pm$ 2 cm s^{-1} (Delcroix *et al.*, 1987), *i.e.* about 50% of the mean zonal geostrophic current in the upper 0-20 m layer and over 100% below 100 m (Fig. 4). Investigating the 0-20 m layer only (where signal/noise ~2), we found a hint that the eastward-flowing geostrophic current, averaged within 26°S-18°S, diminished by about 2 cm s^{-1} during a 1-year period, one year after the 1982-1983 and 1987 El Niño. Such a decrease is consistent with the southward displacement of the anticyclonic gyre axis observed during the 1982-83 El Niño (Delcroix and Hénin, 1989). However, the 2 cm s^{-1} decrease did not appear in 1992 and, furthermore, no increase was detectable during the 1988 La Niña. Hence, given the weakness of the possible ENSO-related signal (~2 cm s^{-1}) and considering that the interannual anomalies of zonal geostrophic current (not shown here) are not significantly correlated with the SOI ($R < 0.5$), this precludes a definite conclusion as to whether or not the zonal geostrophic circulation is systematically affected by ENSO in the studied region.

CONCLUSION AND DISCUSSION

In this paper, an attempt was made to identify the signature of ENSO in oceanic and wind data collected for years in the south western Pacific (17°S-27°S; 160°E-170°E), within an area centred on New Caledonia. This region is of interest since past studies indicated that it presents ENSO-related anomalies out of phase with most of the other regions of the globe. Following a detailed analysis of long-term means and seasonal changes, the link between ENSO and anomalies in SST, SSS, 0-400 m temperature and zonal geostrophic current, and surface wind (τ) was investigated through comparisons with the Southern Oscillation Index (SOI).

During the warm phase of ENSO (SOI < 0; El Niño), we observed saltier-than-average SSS anomalies, cold temperature anomalies that extended at least to 50 m depth, together with westerly and southerly wind anomalies over a large part of the studied area. Interestingly, anomalies of opposite sign were detected during the cold phase of ENSO (SOI > 0; La Niña). We must however bear in mind that the ENSO-signals are relatively weak: the ranges of the interannual SST and τ anomalies are only 20-30% of the corresponding mean seasonal ranges. The exception is for SSS which experiences ENSO-related anomalies of similar magnitude as, or greater than, the mean seasonal changes. Furthermore, SSS anomalies are not in phase with the SOI, unlike SST and τ anomalies, but rather present a time lag that increases from 8 months at 17°S to 13 months at 27°S (SSS after SOI). It was also noted that SST and SSS anomalies do exist inside the lagoon of New Caledonia. Modification of the zonal geostrophic circulation in relation

to ENSO was not ascertained, mainly due to the weakness of possible related anomalies *versus* the accuracy of the calculated geostrophic current.

We shall now propose tentative explanations for the observed regional ENSO-related anomalies. During the warm phase of ENSO (El Niño, SOI < 0), the Warm Pool with SST warmer than 28-29 °C is displaced from the western to the central equatorial Pacific (Picaut and Delcroix, 1995). Lowering pressure in the central equatorial Pacific produces anomalous Walker and Hadley circulation, and, as a conceivable consequence, the regional SE geostrophic trade winds veer clockwise, generating the observed westerly and southerly wind anomalies. The reverse situation appears during the cold phase of ENSO (La Niña, SOI > 0) when the warm pool is displaced toward the far western equatorial Pacific. Regarding near-surface temperature fluctuations, they can be due to anomalies in air-sea heat exchange and/or to modifications in heat transport by anomalous ocean currents. These two mechanisms, which cannot be rigorously quantified with our data set, may work in concert during both phases of ENSO. In fact, the cold temperature anomalies during the warm phase are consistent with: 1) an increase in the wind speed (τ) which induces evaporative cooling (Meyers *et al.*, 1986); 2) the occurrence of southerly wind anomalies bringing dryer and cooler air from the south; and 3) the import of relatively cold water coming from the east due to both anomalous westward Ekman transport related to southerly wind anomalies and possibly to the southern displacement of the large-scale anticyclonic gyre axis (Wyrtki and Wenzel, 1984; Delcroix and Hénin, 1989, their Fig. 12). The warm near-surface temperature anomalies during the cold phase of ENSO are in accord with the reverse processes. As for SSS anomalies, saltier-than-average SSS during the warm phase of ENSO are remarkably consistent with the reduced precipitation observed 9 to 13 months after the peak SOI in the region of New Caledonia (Ropelewski and Halpert, 1987; their Fig. 3*d*). Of possible importance is also the enhanced evaporation due to an increase in the wind speed, as well as the income of saltier water from the east in response to the circulation change just discussed above. The 8-13 months delay between the SSS anomalies and the SOI suggests, however, that these anomalies are mainly governed by precipitation changes.

Hence, there is no doubt that ENSO is one of the major factors influencing interannual climate variations in the vicinity of New Caledonia. We have suggested several consistent causes that can account for the regional ENSO-related anomalies, and that connect these anomalies to ENSO evolution at low-latitudes. Model simulations and/or altimetric measurements should provide the complementary information needed to assess and/or to discriminate the relative magnitude of the mechanisms identified.

Acknowledgements

Special thanks go to the many ORSTOM scientists and/or colleagues involved in the collection of data gathered under the ship-of-opportunity programme and oceanic cruises. The FSU wind data was supplied by James J. O'Brien and co-workers. We wish to thank Christian Hénin and Pierre Rual for their suggestions and helpful comments during the course of this study. For one of us (OL), this investigation is part of a *Mémoire de Diplôme d'Études Approfondies de l'Université d'Aix-Marseille-II*, and a *Mémoire de Stage de l'École Supérieure d'Ingénieurs de Marseille*, performed while visiting the ORSTOM Center in Nouméa. Support from this Institute has been greatly appreciated.

REFERENCES

Bendat J., A. Piersol (1971). Random Data: analysis and measurement procedures. Wiley-Interscience, 407 p.

Berlage H.P. (1966). The Southern Oscillation and world weather. *K. Ned. Met. Inst., Meded. Verh.* **88**, 152 p.

Bjerknes J. (1966). A possible response of the atmospheric Hadley circulation to equatorial anomalies of ocean temperature. *Tellus* **18**, 820-829.

Cadet D. (1985). The Southern Oscillation over the Indian Ocean. *J. Climatol.* **5**, 189-212.

Delcroix T., G. Eldin, C. Hénin (1987). Upper ocean water masses and transports in the western tropical Pacific (165°E). *J. Phys. Oceanogr.* **17**, 2248-2262.

Delcroix T., C. Hénin (1989). Mechanisms of subsurface thermal structure and sea surface thermohaline variabilities in the southwestern tropical Pacific during 1979-1985. *J. Mar. Res.* **47**, 777-812.

Delcroix T., C. Hénin (1991). Seasonal and interannual variations of sea-surface salinity in the tropical Pacific Ocean. *J. Geophys. Res.* **96**, 22135-22150.

Delcroix T. (1993). Seasonal and interannual variability of sea-surface temperatures in the tropical Pacific, 1969-1991. *Deep-Sea Res.* **40**, 2217-2228.

Delecluse P., J. Servain, C. Levy, K. Arpe, L. Bengtsson (1994). On the connection between the 1984 Atlantic warm event and the 1982-1983 ENSO. *Tellus* **46**, 448-464.

Donguy J.R. (1987). Recent advances in the knowledge of the climatic variations in the tropical Pacific Ocean. *Prog. Oceanogr.* **19**, 49-85.

Goldenberg S., J. O'Brien (1981). Time and space variability of tropical wind stress. *Mon. Weather Rev.* **109**, 1190-1207.

Gordon N. (1986). The Southern Oscillation and New Zealand weather. *Mon. Weather Rev.* **114**, 371-387.

Halpert M., C. Ropelewski (1992). Surface temperature patterns associated with the Southern Oscillation. *J. Climate* **5**, 577-593.

Hanawa K., P. Rual, R. Bailey, A. Sy, M. Szabados (1994). Calculation of new depth equations for expendable bathythermograph using a temperature-error-free method (Application to Sippican/TSK T-7, T-6 and T-4 XBTs). IOC technical series 42, UNESCO.

Hénin C. (1982). Caractéristiques des températures et salinités de surface et leurs variabilités dans le Pacifique sud-ouest. Rapports Scientifiques et Techniques, Centre ORSTOM de Nouméa, Nouvelle Calédonie, **28**, 18 p.

Hénin C., J.M. Guillerm, L. Chabert (1984). Circulation superficielle autour de la Nouvelle Calédonie. *Océanogr. Trop.* **19**, 113-126.

Hénin C., F. Gallois, M.J. Langlade (1995). Rapport des données physiques de la campagne ZoNéCo-2 à bord du N.O. L'ATALANTE du 2 au 21 août. Rapports de missions, Sciences de la mer, Océanographie physique, Centre ORSTOM de Nouméa, Nouvelle Calédonie, **15**, 40 p.

Hildebrandsson H.H. (1897). Quelques recherches sur les centres d'action de l'atmosphère. *Kongl. Svenska Vetenskaps-Akademiens Handlingar.*, Bandet 29, **3**, 36 p.

Lenormand O. (1995). Les anomalies climatiques associées à ENSO ont-elles une influence au voisinage de la Nouvelle Calédonie ? Mémoire de DEA, sciences de la mer, océanographie physique, centre ORSTOM de Nouméa, 52 p.

Lukas R., P. Webster (1992). TOGA-COARE, Tropical Ocean Global Atmopshere program and Coupled Ocean Atmosphere Response Experiment. *Oceanus* **35**, 62-65.

McCreary J., D. Anderson (1991). An overview of coupled ocean-atmosphere models of El Niño and the Southern Oscillation. *J. Geophys. Res.* **96** suppl., 3125-3151.

Merle J., H. Rotschi, B. Voituriez (1969). Zonal circulation in the tropical western south Pacific. In: *"Perspectives in Fisheries Oceanography". Jap. Soc. Fish. Oceanogr.*, Prof. Uda's special number, 91-98.

Meyers G., J.R. Donguy (1980). An XBT network with merchant ships. *Trop. Ocean-Atmos. Newslett.* **2**, 6-7.

Meyers G., J.R. Donguy, R.K. Reed (1986). Evaporative cooling of the western equatorial Pacific Ocean by anomalous winds. *Nature* **323**, 523-526.

Morlière A., J.P. Rébert (1986). Rainfall shortage and El Niño Southern Oscillation in New Caledonia, southwestern Pacific. *Mon. Weather Rev.* **114**, 1131-1137.

Picaut J., T. Delcroix (1995). Equatorial wave sequence associated with the warm pool displacement during the 1986-1989 El Niño and La Niña. *J. Geophys. Res.* **100**, 18398-18408.

Rasmusson E.M., T.H. Carpenter (1982). Variations in tropical sea surface temperature and surface wind field associated with the Southern Oscillation/El Niño. *Mon. Weather Rev.* **110**, 354-384.

Ropelewski C. F., M. S. Halpert (1987) Global and regional scale precipitation patterns associated with the El Niño/Southern Oscillation. *Mon. Weather Rev.* **115**, 1606-1626.

Rougerie F., J.R. Donguy (1975). La mer du Corail en régime d'alizé de sud-est. *Cah. ORSTOM, sér. Océanogr.* **13**, 49-67.

Tomczak M. (1981). Bass Strait water intrusions in the Tasman Sea and mean temperature-salinity curves. *Aust. J. Mar. Freshwater Res.* **32**, 699-708.

Trenberth K., T. Hoar (1996). The 1990-1995 El Niño Southern oscillation event: longest on record. *Geophys. Res. Let.* **23**, 57-60.

van Loon H., Shea J. (1985). The Souther Oscillation. IV. The precursors south of 15°S to the extremes of the Oscillation. *Mon. Weather Rev.* **113**, 2063-2074.

Walker G.T. (1923). Correlation in seasonal variations of weather, VIII: a preliminary study of world weather. *Mem. Indian Meteor. Dep.* **24**, 75-131.

Walker G.T. (1924). Correlation in seasonal variations of weather, IX: a further study of world weather. *Mem. Indian Meteor. Dep.* **24**, 275-332.

White W., G. Meyers, J.R. Donguy, S. Pazan (1985). Short-term climatic variability in the thermal structure of the Pacific Ocean during 1979-1982. *J. Phys. Oceanogr.* **15**, 917-935.

Wyrtki K. (1962). The subsurface water masses in the western south Pacific Ocean. *Aust. J. Mar. Freshwater Res.* **13**, 18-48.

Wyrtki K. (1975). El Niño - the dynamic response of the equatorial Pacific ocean to atmospheric forcing, *J. Phys. Oceanogr.* **5**, 572-584.

Wyrtki K., J. Wenzel (1984). Possible gyre-gyre interaction in the Pacific ocean. *Nature* **309**, 538-540.